nature research

https://doi.org/10.1038/s41558-020-00963-x

Supplementary information

Zonally contrasting shifts of the tropical rain belt in response to climate change

In the format provided by the authors and unedited

Supplementary Material

Zonally contrasting shifts of the tropical rainbelt in response to climate change

by Mamalakis et al.

Supplementary Table 1: CMIP6 models used in this study and their double-ITCZ biases (in units of probability). For models with multiple runs, the average value of bias across all runs is presented.

	Model	Number of ensembles	Eastern Pacific double-ITCZ Bias	Atlantic double-ITCZ Bias	Average Bias
1	ACCESS-CM2	1	0.48	0.54	0.50
2	ACCESS-ESM1-5	3	0.36	0.20	0.31
3	BCC-CSM2-MR	1	0.53	0.60	0.55
4	CAMS-CSM1-0	2	0.53	0.85	0.64
5	CanESM5	20	0.35	0.70	0.46
6	CanESM5-CanOE	3	0.36	0.71	0.47
7	CESM2	6	0.23	0.40	0.29
8	CESM2-WACCM	1	0.22	0.46	0.30
9	CNRM-CM6-1	6	0.32	0.51	0.38
10	CNRM-CM6-1-HR	1	0.28	0.50	0.35
11	CNRM-ESM2-1	5	0.35	0.51	0.40
12	FGOALS-f3-L	1	0.22	0.37	0.27
13	FGOALS-g3	1	0.31	0.42	0.34
14	GFDL-ESM4	1	0.49	0.72	0.57
15	GISS-E2-1-G	1	0.53	0.78	0.61
16	INM-CM4-8	1	0.44	0.77	0.55
17	INM-CM5-0	5	0.43	0.67	0.51
18	IPSL-CM6A-LR	11	0.19	0.74	0.38
19	KACE-1-0-G	3	0.47	0.39	0.45
20	MIROC6	3	0.16	0.38	0.24
21	MIROC-ES2L	1	0.22	0.53	0.32
22	MPI-ESM1-2-HR	10	0.34	0.83	0.50
23	MPI-ESM1-2-LR	10	0.29	0.85	0.48
24	MRI-ESM2-0	1	0.26	0.58	0.36
25	NorESM2-LM	1	0.39	0.51	0.43
26	NorESM2-MM	1	0.21	0.29	0.23
27	UKESM1-0-LL	5	0.30	0.48	0.36

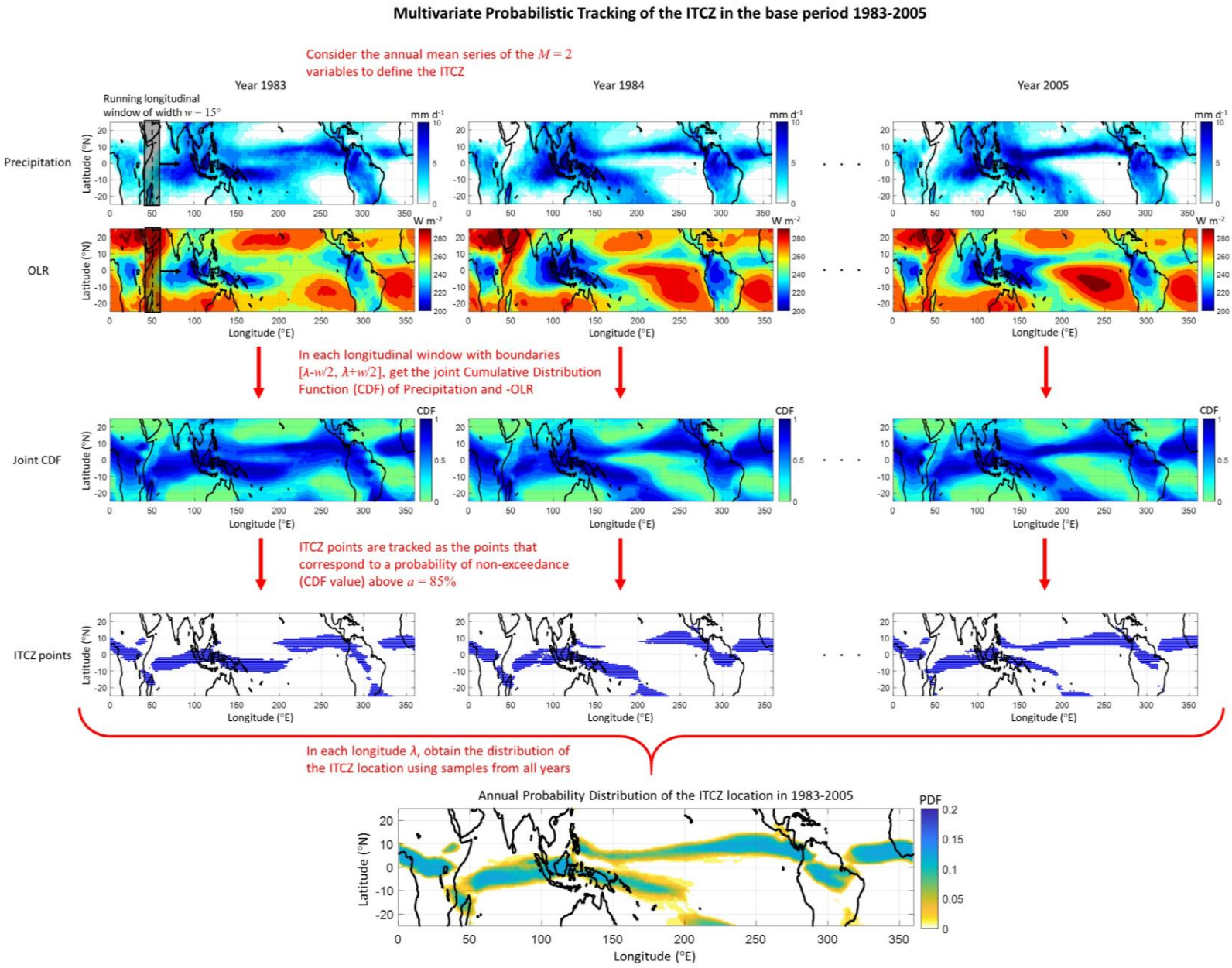

Supplementary Figure 1: Application of a longitudinally explicit, multivariate probabilistic approach to track the ITCZ on annual scales. The approach is shown here for the case when the defining variables are M = 2, i.e. precipitation and outgoing longwave radiation (OLR); we use satellite data (see data availability statement), and the tracking probability threshold is a = 85%. When aiming to track the ITCZ on seasonal scales, only the season of interest is used from each year. For more information, please see section *Methods*, and Mamalakis and Foufoula-Georgiou (2018).

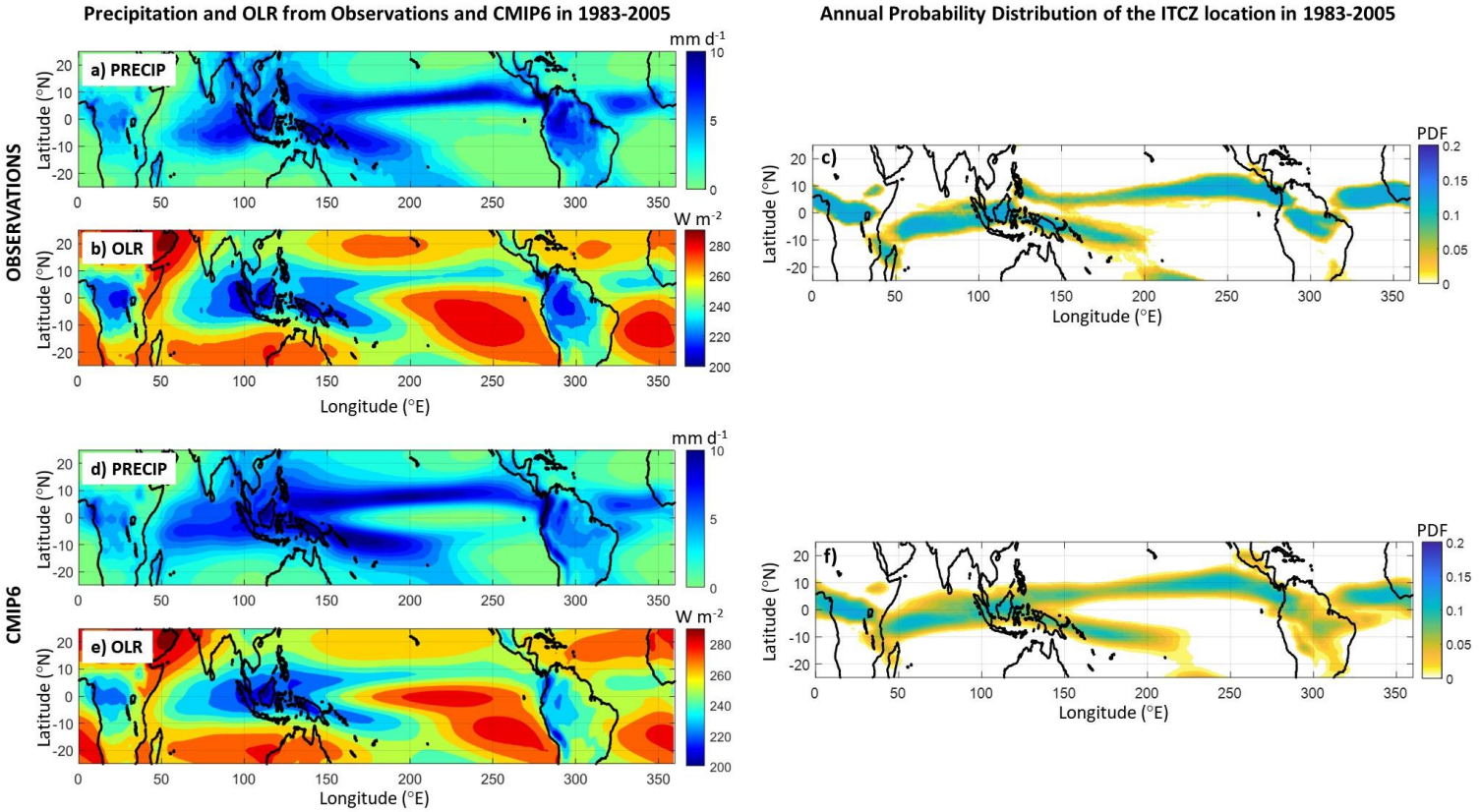

Supplementary Figure 2: The baseline climatology of the ITCZ in observations and CMIP6, as shown in average precipitation and OLR maps, and using a multivariate probabilistic tracking framework. a) Observed multi-year mean tropical precipitation in 1983-2005. b) Same as in (a), but for outgoing longwave radiation (OLR). c) Probability density function (PDF) of the location of the ITCZ on annual scales and in all longitudes. The ITCZ tracking is performed based on the joint statistics of the observed window-mean precipitation and outgoing longwave radiation (OLR) in overlapping longitudinal windows (see Supplementary Figure 1 and section *Methods*). d-f) Same as in (a-c), but results are obtained from the CMIP6 output. The multi-model mean across 27 CMIP6 is presented.

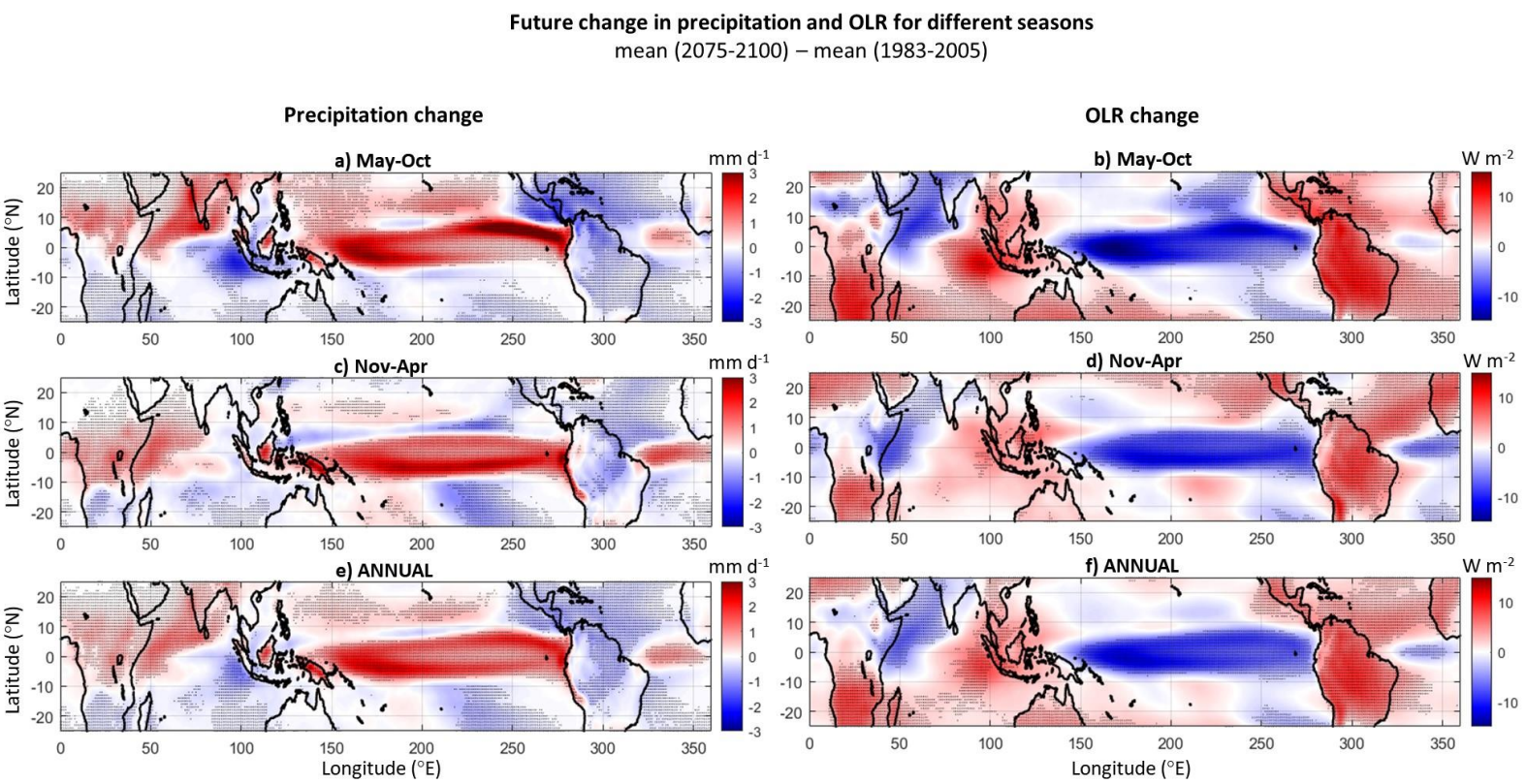

Supplementary Figure 3: Future changes in mean precipitation and outgoing longwave radiation in response to climate change, as projected by CMIP6 models. a) Difference in the May-Oct seasonal mean precipitation between 2075-2100 and 1983-2005. b) Same as in (a), but for outgoing longwave radiation (OLR). c-d) Same as in (a-b), but for Nov-Apr. e-f) Same as in (a-b), but annual mean changes are presented. In all plots, the multi-model mean across 27 CMIP6 models is presented, while stippling indicates agreement (in the sign of the change) in more than ¾ of the models considered.

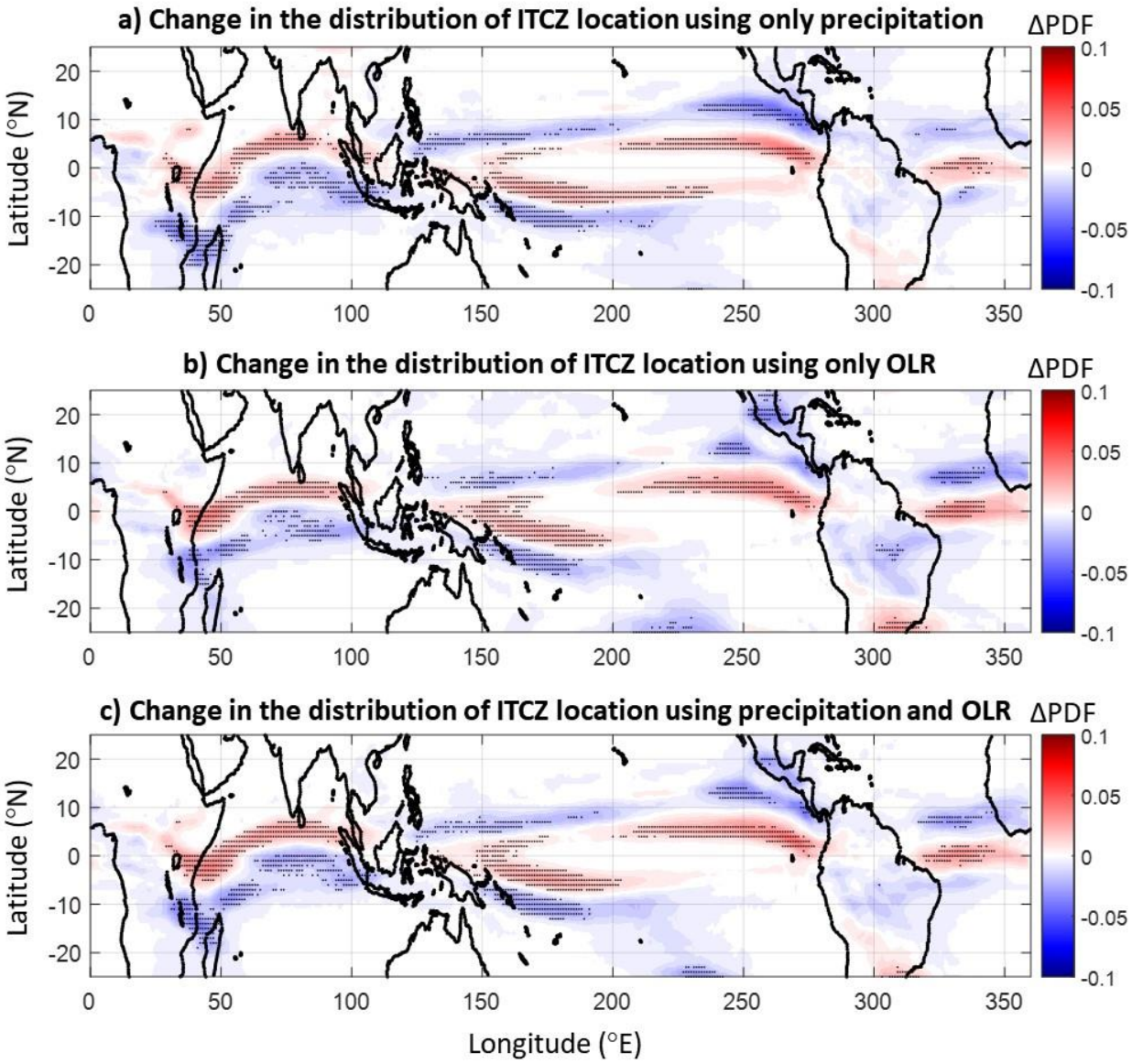

Supplementary Figure 4: Future changes in the ITCZ location in CMIP6 using the multivariate probabilistic tracking framework. a) Difference in the annual probability density function (ΔPDF) of the location of the ITCZ between 2075-2100 and 1983-2005. The ITCZ tracking is performed using only precipitation. b) Same as in (a), but outgoing longwave radiation (OLR) is used to track the ITCZ. c) Same as in (a), but both precipitation and OLR are jointly used to track the ITCZ (see Supplementary Figure 1 and section *Methods*); this panel is identical with Figure 1c. In all plots, the multi-model mean across 27 CMIP6 models is presented, while stippling indicates agreement (in the sign of the change) in more than ¾ of the models considered. All plots show (to a greater or lesser extend) a northward ITCZ shift over eastern Africa and Indian Ocean and a southward ITCZ shift over the eastern Pacific, South America, and the Atlantic.

Supplementary Discussion

Climatology of the ITCZ and model biases

Here, we explore the ability of the considered CMIP6 climate models in accurately reproducing the recent ITCZ climatology and interannual variability. In doing so, we compare the distributions of the location of the ITCZ in May-Oct and Nov-Apr (during the base period 1983-2005) as derived by using satellite observations with those derived by using model outputs (for information on the ITCZ tracking approach, see Supplementary Figures 1-2, section *Methods*, and Mamalakis and Foufoula-Georgiou, 2018). The analysis of observations indicates that during May-Oct, the ITCZ is a zonally oriented feature located mainly in the Northern Hemisphere, apart from the Indian Ocean (see Supplementary Figure 5a), where a secondary ITCZ also prevails in the equator associated with the so-called "equatorial jump" (Pauluis, 2004), and the western Pacific, where the tropical part of the south Pacific convergence zone (SPCZ) is also tracked by our method. In the Nov-Apr period, the ITCZ migrates to the south (mainly over land; see Supplementary Figure 5c), and three southern convergence features strengthen: the SPCZ (Haffke and Magnusdottir, 2013), the south Atlantic convergence zone (SACZ; Carvalho et al., 2004), and the south Indian ocean convergence zone (SIOCZ; Cook, 1998; 2000), which, in contrast to the summer ITCZ, are diagonally oriented (Widlansky et al., 2011; Barimalala et al., 2018). The highest intra-annual variability of the ITCZ location is found in the western and central Pacific (Mamalakis and Foufoula-Georgiou, 2018), where the ITCZ consists of two distinct and much distant zones, the SPCZ and the northern ITCZ. These two bands coexist for most of the year, with the SPCZ strengthening during boreal winter and the northern ITCZ strengthening during boreal summer (see Figure 2 of Waliser and Gautier, 1993; Widlansky et al., 2011; Berry and Reeder, 2014; Haffke and Magnusdottir, 2013, 2015). The smallest intra-annual variability of the ITCZ location is found in the eastern Pacific and Atlantic oceans, where the ITCZ tends to stay in the northern hemisphere during most of the year; however a double ITCZ may form in the eastern Pacific during boreal spring (see Supplementary Figure 5c and Adam et al., 2016b; Bischoff and Schneider, 2016; Haffke et al., 2016; Yang and Magnusdottir, 2016).

Although CMIP6 models are mostly consistent in simulating the location of the ITCZ during May-Oct, they exhibit important biases in the Pacific and Atlantic oceans during Nov-Apr (see Supplementary Figures 5-6). Particularly, models tend to overestimate the probability of the ITCZ migrating to the southern hemisphere over the eastern Pacific and Atlantic Oceans. These biases have been well documented in the literature (the so-called "double-ITCZ biases", see Mechoso et al., 1995; Oueslati and Bellon, 2015) and explored as to their linkage with other systematic biases in simulated equatorial sea surface temperatures and the atmospheric energy input/transport (Hwang and Frierson, 2013; Li and Xie, 2014; Oueslati and Bellon, 2015; Adam et al., 2016a; Adam et al., 2018; Tian and Dong, 2020).

Due to these biases, projections of future ITCZ shifts, which are usually obtained as the difference between the simulated future and baseline averages, need to be cautiously interpreted and analyzed. Particularly, including information about the present-day ITCZ model biases in the analysis may lead to a better understanding of future ITCZ shifts, as recent literature suggests (Dutheil et al., 2019; Samanta et al., 2019). In order to assess the impact of these present-day model biases on our interpretation of the future ITCZ trends more quantitatively, we calculated the average difference in the (Nov-Apr) probability distribution of the ITCZ location between models and observations over specific boxes (see Supplementary Figure 6a and section *Methods* for more information). Our results indicated that CMIP6 models simulate a more frequent southward migration of the Atlantic ITCZ than what is observed, by $\Delta P = 57 \pm 17.8\%$ (that is the spatially-

averaged difference in probability between models and observations over tropical Atlantic), and likewise in the Pacific toward the southeastern sector of the basin, by $\Delta P = 34 \pm 11.3\%$ (see Supplementary Figure 6b and Supplementary Table 1). These numbers show that the Atlantic bias is more severe, and as such, the signature of the seasonal double-ITCZ biases on annual scales is apparent mainly over the Atlantic and not so much over the eastern Pacific basin (see Supplementary Figure 5f). Note that when we used the average tropical precipitation and/or OLR difference between models and observations to assess the systematic double-ITCZ biases (i.e. not the probabilistic method), we obtain similar results (see Supplementary Figure 2). Moreover, our analysis shows that there is a statistically significant ($p < 0.05$) positive correlation of eastern Pacific and Atlantic biases across the CMIP6 models on the order of 0.42, which indicates that it may be unlikely for a model to exhibit relatively important biases only in one of the two basins. Apart from the double-ITCZ bias, climate models from both projects are also shown to produce a more zonally oriented SPCZ than what observations suggest (see also Oueslati and Bellon, 2015).

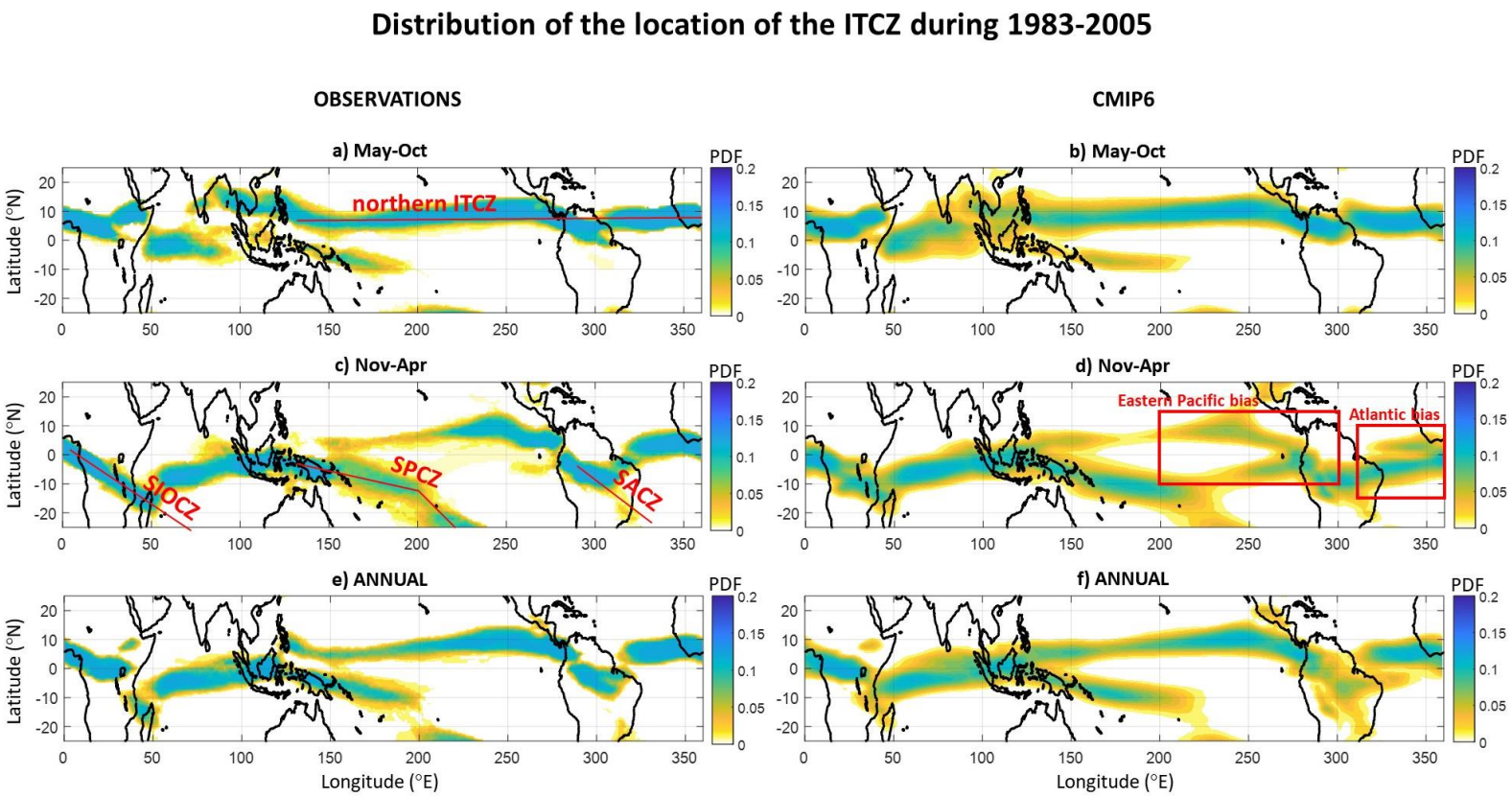

Supplementary Figure 5: Climatological location of the ITCZ during 1983-2005 based on observations and CMIP6 models. a-b) Probability density function (PDF) of the location of the ITCZ in all longitudes during season May-Oct. The ITCZ tracking is performed based on the joint statistics of the observed (panel (a)) or the simulated (panel (b)) window-mean precipitation and outgoing longwave radiation (OLR) in overlapping longitudinal windows (see Supplementary Figure 1 and section *Methods*). c-d) Same as in (a)-(b), but for season Nov-Apr. e-f) Same as in (a)-(b), but tracking is performed on an annual scale. In (b), (d), and (f), the multi-model mean across all 27 CMIP6 models is presented. Some well-known distinct ITCZ features are highlighted in the results from the observations, while the double-ITCZ biases in the eastern Pacific and Atlantic basins are apparent in the CMIP6 results (season Nov-Apr). The areas over which the double-ITCZ biases are quantified are shown as red boxes in panel (d); see section *Methods* for more information.

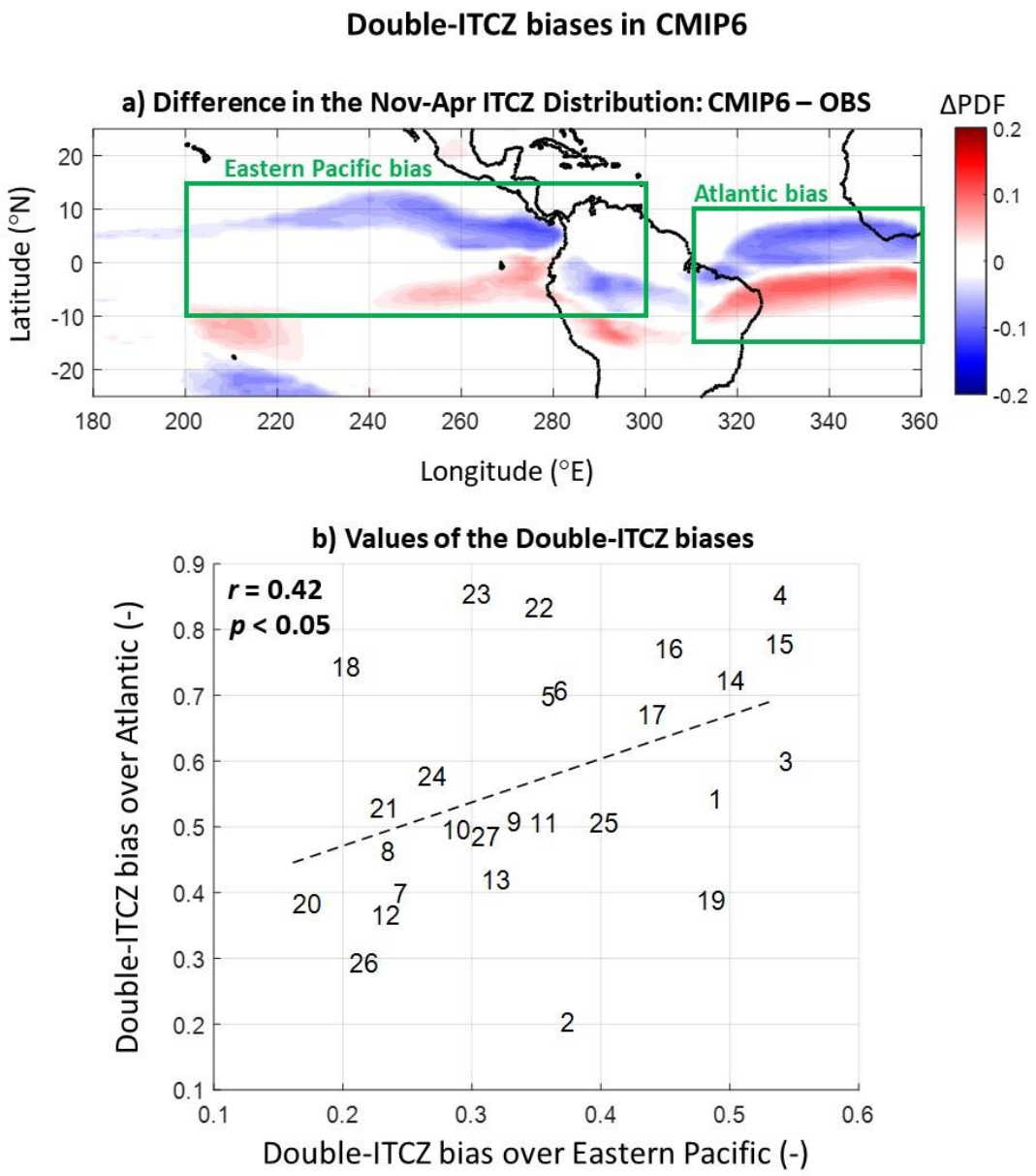

Supplementary Figure 6: Double-ITCZ biases in CMIP6. a) Difference in the distribution of ITCZ location (Nov-Apr) between CMIP6 and observations. The multi-model mean across 27 CMIP6 models is presented. b) Scatter plot of the double-ITCZ biases in CMIP6 models (measured in probability; that is we calculated the average difference in the probability distribution of the ITCZ location between models and observations over the green boxes in panel (a); see section *Methods* for more information). Each model is labeled according to Supplementary Table 1. For models with multiple runs, the average value of bias across all runs is presented. Based on both panels, CMIP6 models are shown to exhibit higher bias over the Atlantic basin than eastern Pacific, while a statistically significant ($p < 0.05$) positive dependence ($r = 0.42$) of these biases is apparent in panel (b). The latter indicates that it may be unlikely for a model to exhibit relatively important bias only in one of the two ocean basins.

To explore the ability of the models to accurately simulate the ITCZ on interannual time scales, we compared the effect of the El Niño – Southern Oscillation (ENSO) on the location of the ITCZ, as determined by satellite data and model outputs (Supplementary Figure 7). Specifically, we calculated the difference in the distribution of the ITCZ location between years corresponding to the

four strongest El Niño events and the four strongest La Niña events during the 23-yr base period 1983-2005. In models runs, El Niño and La Niña events do not correspond to the same years with reality, thus, we used the Niño 3.4 index to define ENSO events. Results show that CMIP6 models are mostly consistent in reproducing the effect of ENSO on the location of the ITCZ during Nov-Apr (the period when ENSO typically peaks). Results from both the observations and the models indicate that during El Niño conditions, the ITCZ is displaced more equatorward in the Pacific relative to La Niña conditions, due to the anomalous heating in the tropical Pacific Ocean which favors deep convection (Dai and Wigley, 2000; Berry and Reeder, 2014, Adam et al., 2016b).

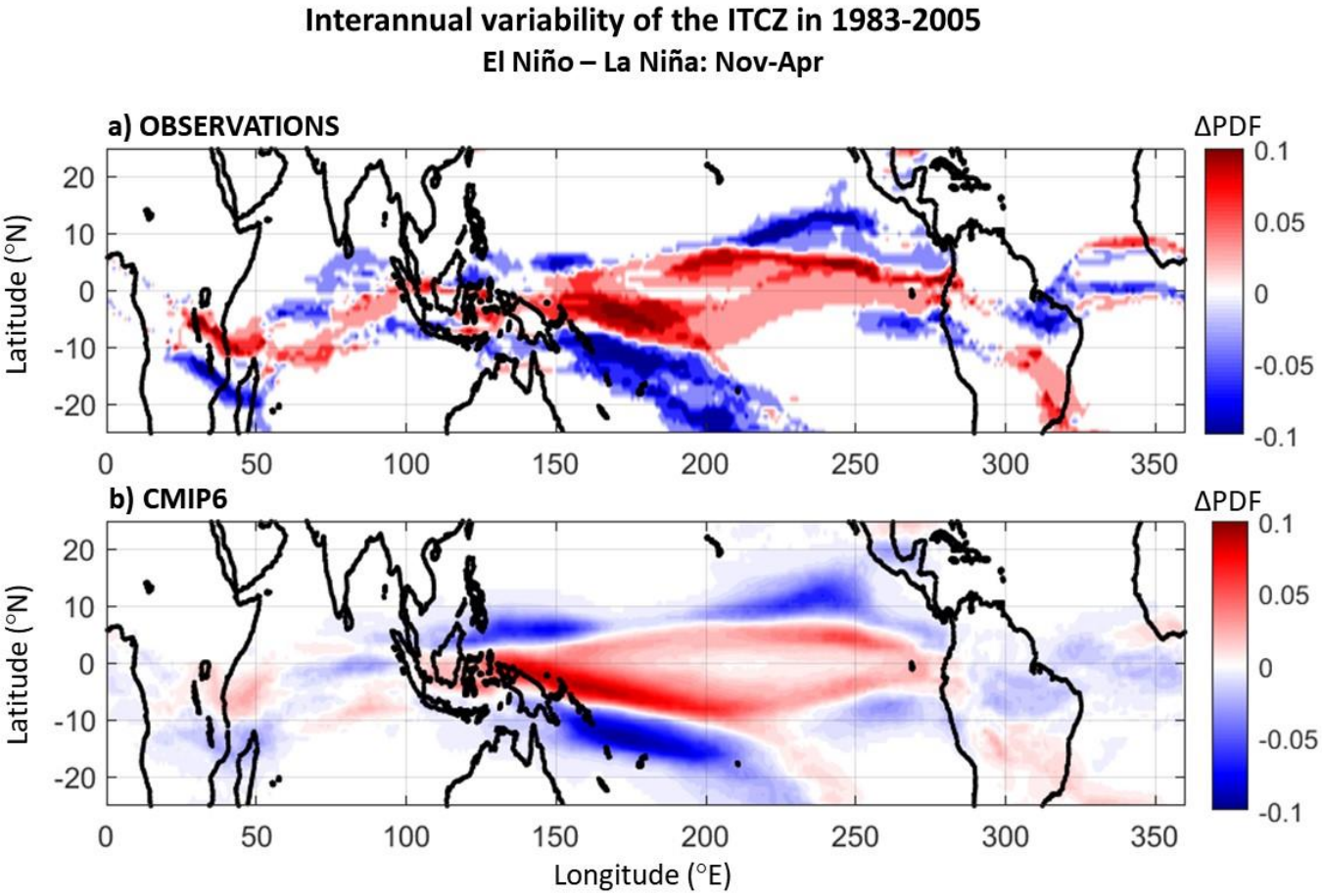

Supplementary Figure 7: The effect of El Niño-Southern Oscillation on the location of the ITCZ during season Nov-Apr. a) Difference in the distribution of the ITCZ location between the four strongest El Niño years and the four strongest La Niña years in the observational record in 1983-2005 (the Niño 3.4 index is used to define the El Niño state). It is shown that during El Niño years, the ITCZ is located more equatorward in the Pacific. b) Same as in (a), but the multi-model mean across 27 CMIP6 models is presented, revealing that CMIP6 models capture quite consistently the ENSO effect on the ITCZ.

With regard to the effect of the double-ITCZ biases on the revealed, zonally-contrasting, ITCZ response (see main text), we find that the results over the Eurasian sector are not sensitive to the performance of the models in the base period. That is, there is no statistically significant relationship between the double-ITCZ biases and the projected shift over the Eurasian sector across CMIP6 models (not shown). However, over the eastern Pacific – Atlantic sector (i.e. where the double-ITCZ biases occur), the double-ITCZ biases seem to influence the sign of the predicted ITCZ

shift to some extent. In particular, our analysis shows that the smaller the bias of a model over the southern Atlantic, the more likely it is to predict a southward shift of the Atlantic ITCZ in the future (see Supplementary Figure 8). This implies that the pattern of the ITCZ contraction over the Atlantic Ocean that is depicted in e.g. Figure 1 is likely a spurious result, originating from some of the models being highly biased during the base period. Since in reality the Atlantic ITCZ remains in the northern hemisphere for most of the year (see Supplementary Figures 2,5), a future southward Atlantic ITCZ shift as indicated by the models with lower bias is more likely, which is driven by enhanced sea surface warming over the equator of the basin (see Figure 3 and discussion in main text). Instead, since there is very little to zero precipitation over the southern Atlantic Ocean, a future negative pattern of ITCZ change over the southern Atlantic Ocean as shown in e.g. Figure 1b is an artifact from the high bias in some models and will be an algebraic impossibility in reality. In support of this interpretation, we find that the small number of CMIP6 models that predict a northward ITCZ shift over the eastern Pacific – Atlantic sector (i.e. in contrast to the majority of the models that predict a southward ITCZ shift; see Figure 2b) exhibit relatively high double-ITCZ biases in the base period. Thus, we argue that the double-ITCZ biases, if anything, are obscuring the full extent of the southward ITCZ shift over the eastern Pacific – Atlantic sector, and thus, our result of the zonally contrasting response of the ITCZ to climate change (see main text) is on the conservative side.

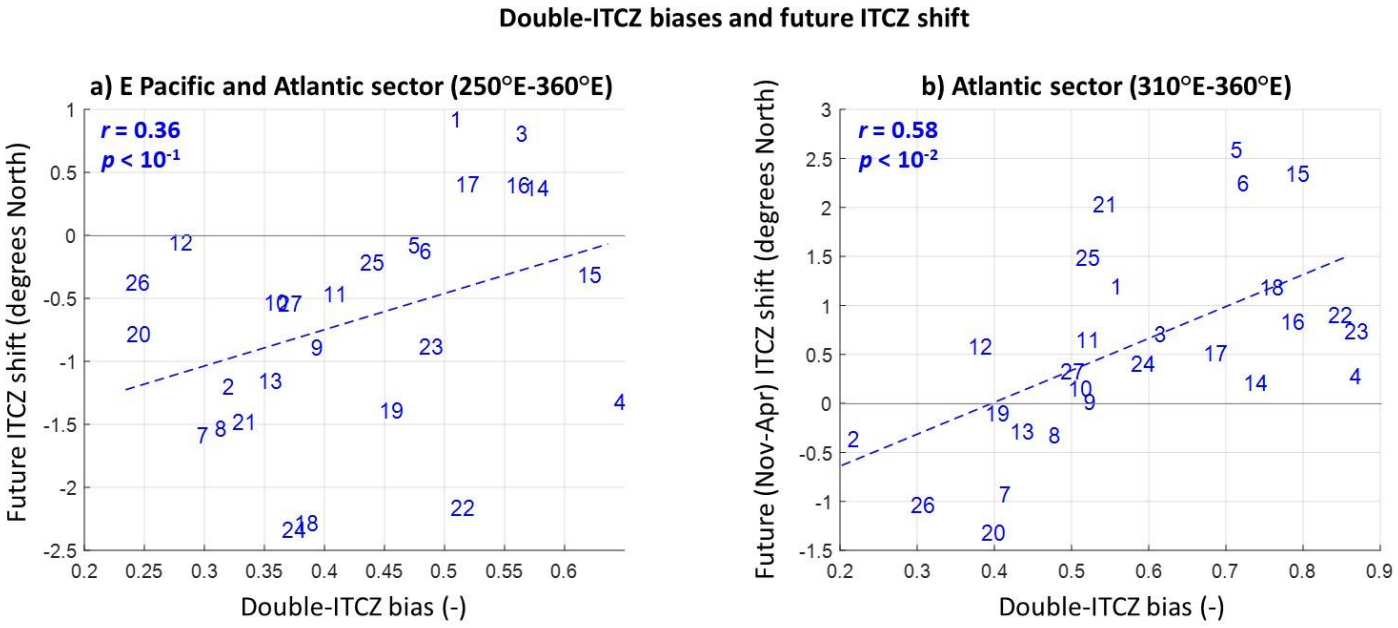

Supplementary Figure 8: The effect of the double-ITCZ bias on the sign of the projected ITCZ shift over the eastern Pacific – Atlantic sector. a) The ITCZ shift (in degrees of latitude; positive implies a northward shift) over the eastern Pacific – Atlantic sector between 2075-2100 and 1983-2005 is shown as a function of the double-ITCZ bias for all CMIP6 models (measured in probability; that is we calculated the average difference in the probability distribution of the ITCZ location between models and observations over the green boxes in Supplementary Figure 6a). Each model is labeled according to Supplementary Table 1. For models with multiple runs, the average value of the shift or the bias across all runs is presented. b) Same as in (a), but results refer to the Atlantic Ocean. In both cases, a statistically significant positive dependence is apparent. This illustrated positive dependence indicates that the lower the double-ITCZ bias of the model over the eastern Pacific – Atlantic sector is in the base period, the more likely it is for the model to project a southward shift of the ITCZ in the future.

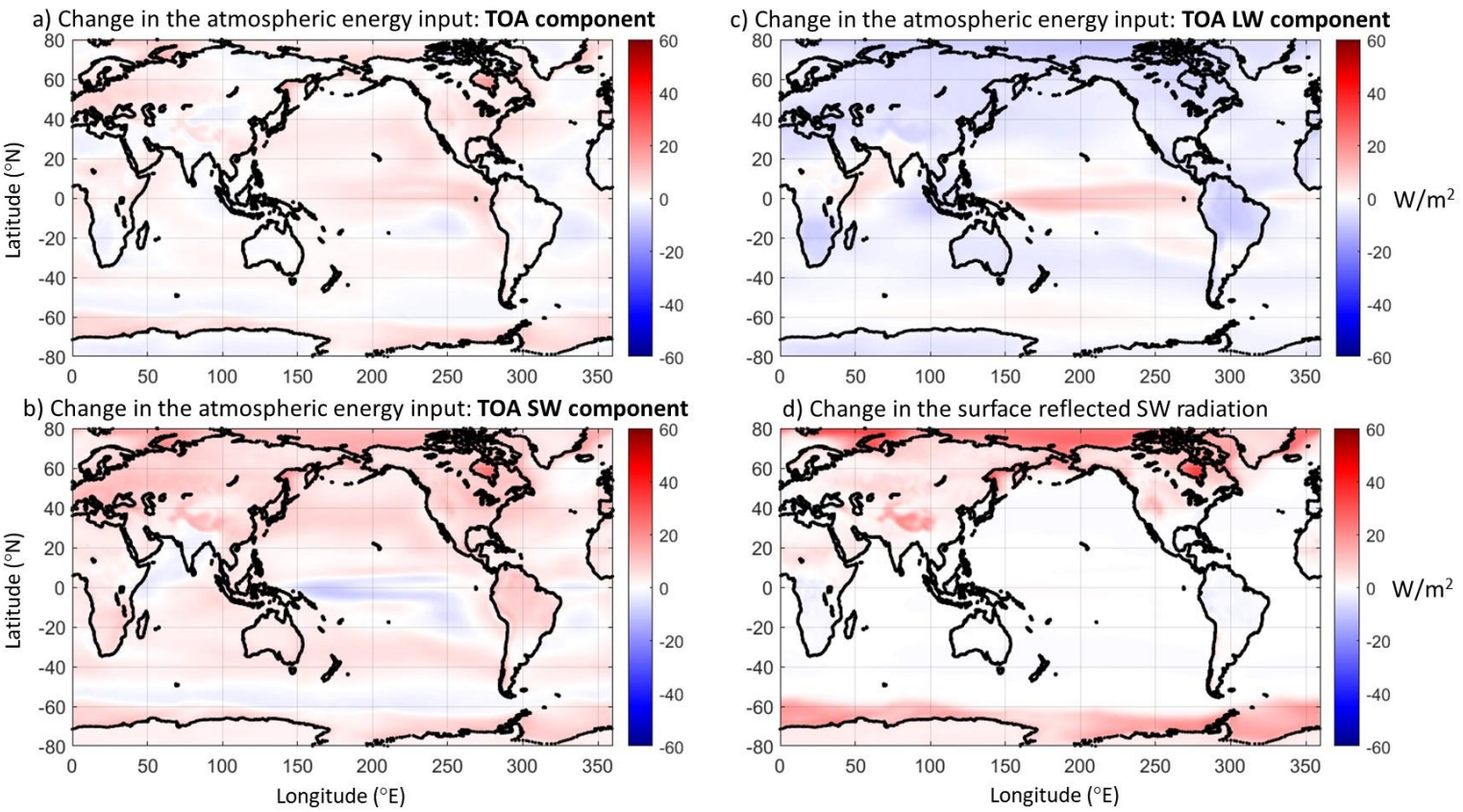

Supplementary Figure 9: Future changes in the components of the atmospheric energy budget, as projected in CMIP6. a) Projected change in the top of the atmosphere (TOA) atmospheric energy input between 2075-2100 and 1983-2005. The multi-model mean across 27 CMIP6 models is presented. b) Same as in (a), but only the TOA shortwave component is presented. c) Same as in (a), but only the TOA longwave component is presented. d) Same as in (a), but the change in the shortwave radiation reaching the surface due to surface albedo changes is presented.

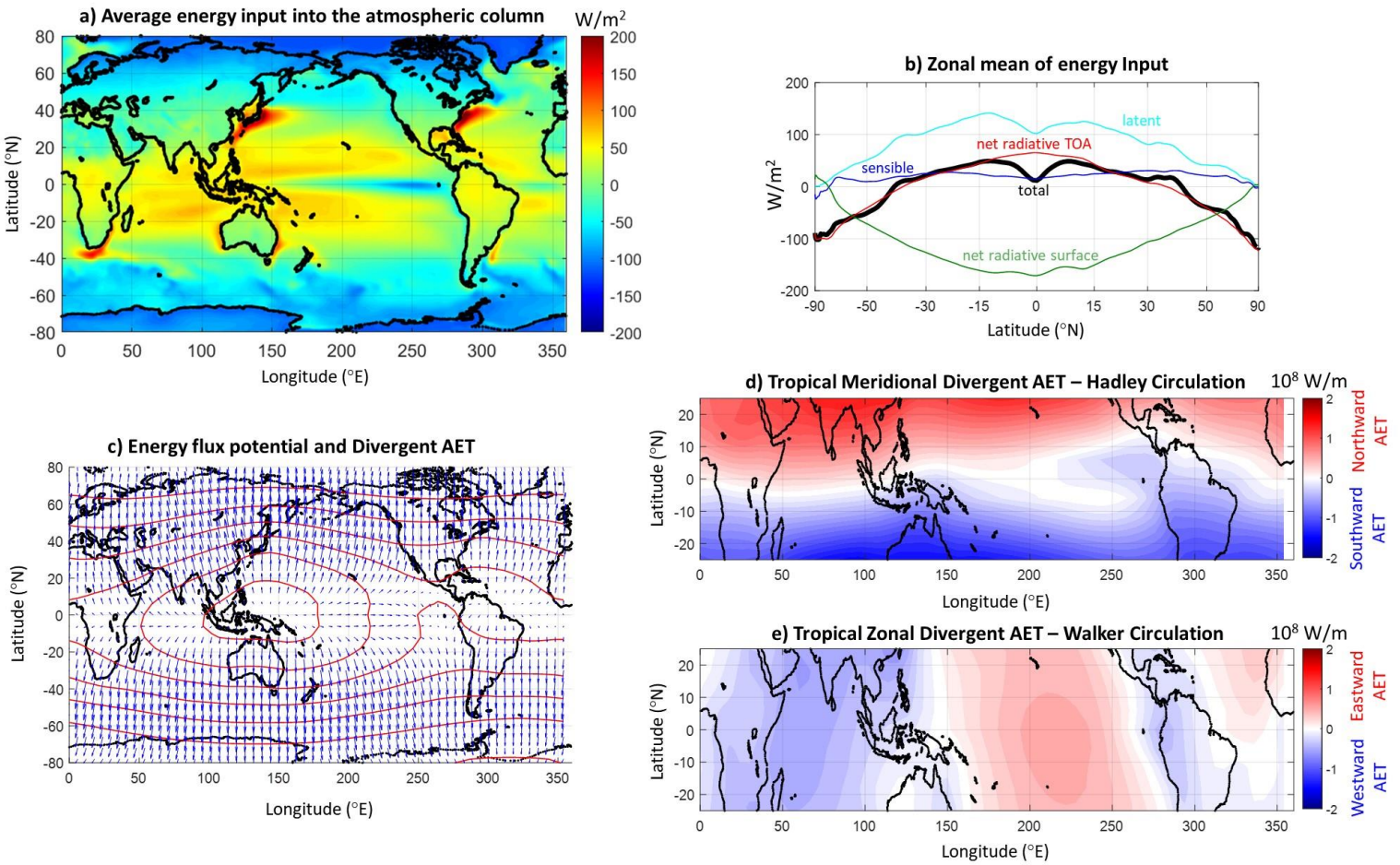

Supplementary Figure 10: Annual-mean atmospheric energy transport in base period 1983-2005, as simulated by CMIP6 models. a) The average energy input (W/m^2) into the atmospheric column in the base period 1983-2005. b) Zonal mean of (a). The horizonal axis is scaled as $\sin(\varphi)$. c) Energy flux potential (red contours; contouring interval is 0.2 PW, with equatorial extrema being minima), and divergent atmospheric energy transport (blue vectors). Vectors are on the order of 10^8 W/m; see panels (d) and (e) for specific values. d) Divergent meridional component of the atmospheric energy transport over the tropics in 1983-2005, most of which is due to the mean meridional atmospheric circulation (Hadley circulation). e) Same as in (d), but the divergent zonal component is presented (it reflects the Walker circulation). In all plots, the multi-model mean across 27 CMIP6 models is presented.

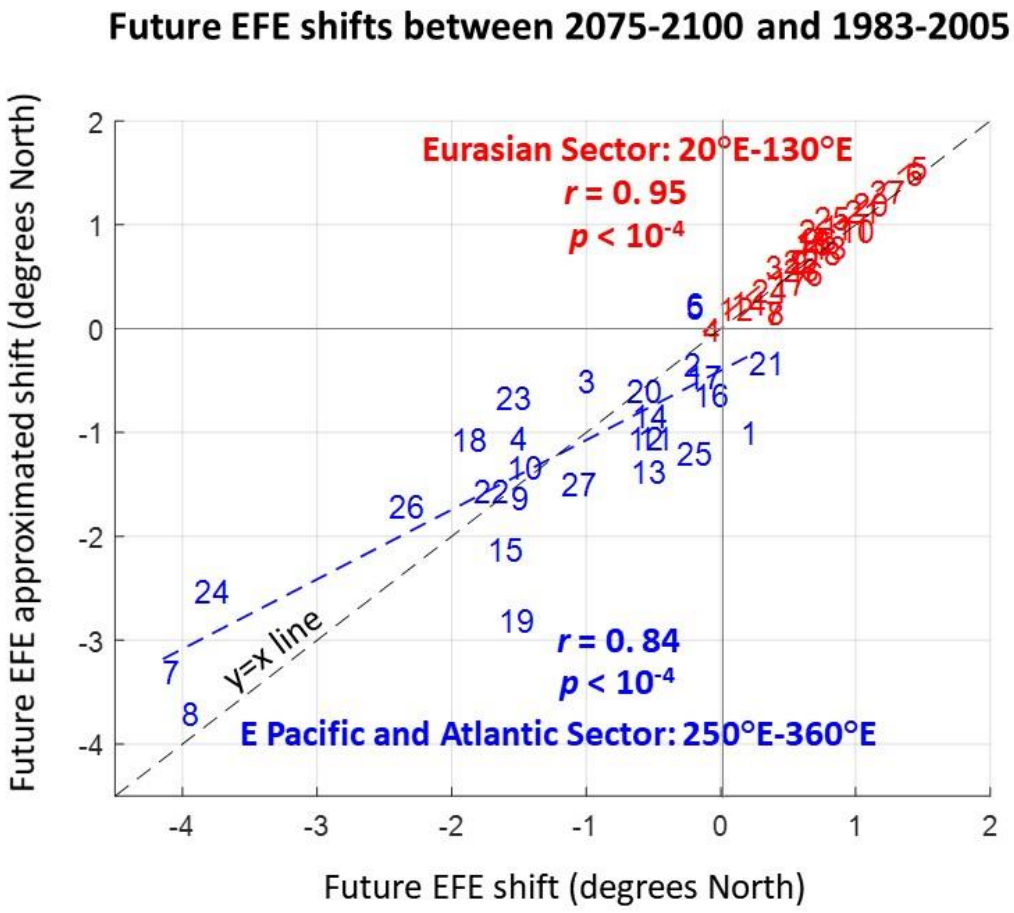

Supplementary Figure 11: Future changes in the energy flux equator (EFE) in response to climate change, as projected by CMIP6 models. Future EFE shifts (between 2075-2100 and 1983-2005) as calculated directly by tracking the latitude where the meridional AET diverges and vanishes (horizontal axis) and approximated EFE shift (using Equation 4 in *Methods*; vertical axis), using all 27 CMIP6 models zonally averaged over the Eurasian sector (20ºE-130ºE; red color) and the eastern Pacific – Atlantic sector (250ºE-360ºE; blue color). Each model is labeled according to Supplementary Table 1. For models with multiple runs, the average value of the shift across all runs is presented. Based on either approach, results show that CMIP6 models project that the EFE will shift northward over the Eurasian sector and southward over the Pacific – Atlantic sector. Also, the agreement between the two approaches is very high especially over the Eurasian sector, which is in accordance with Adam et al. (2016b); see their Figure 5.

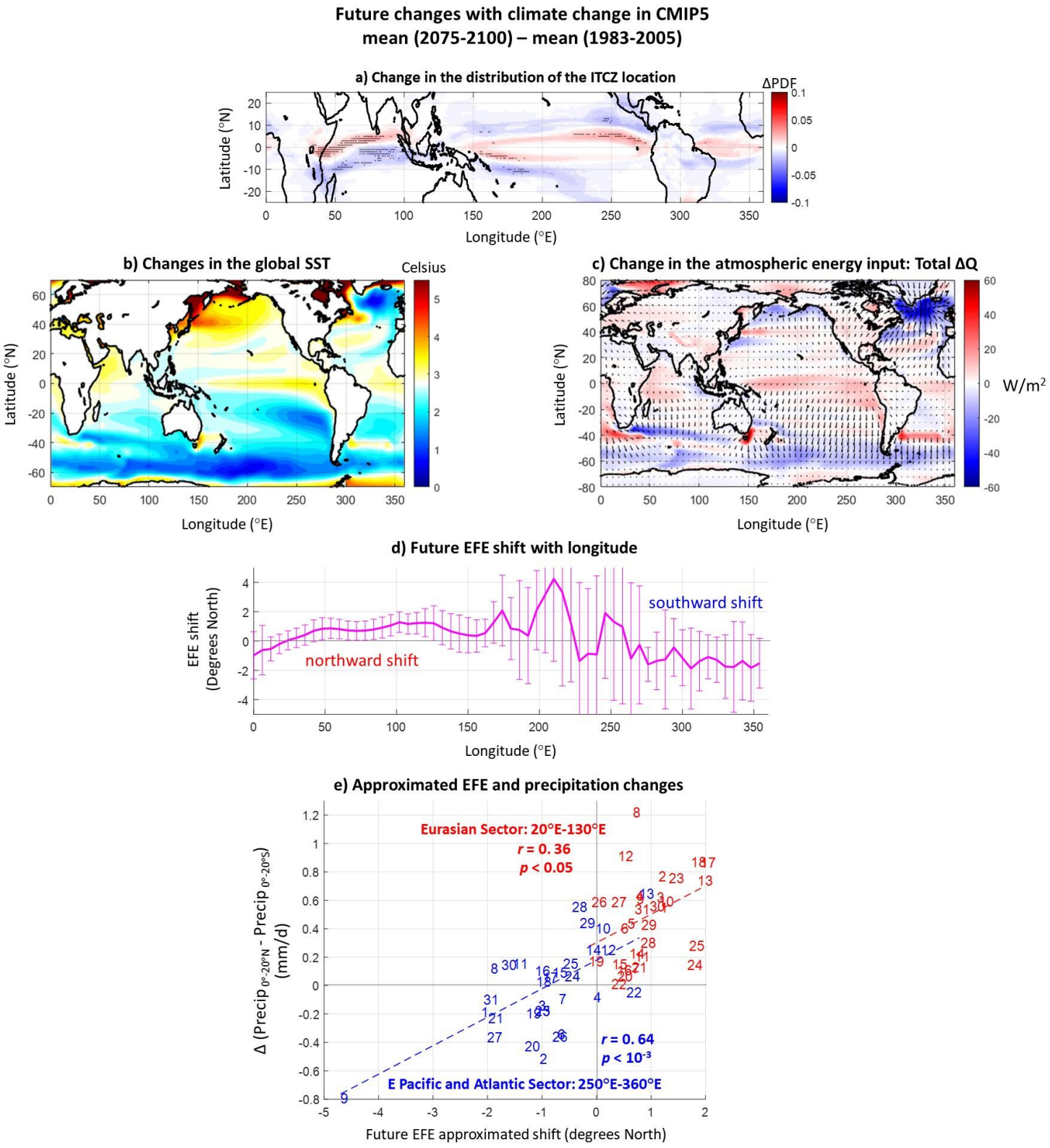

Supplementary Figure 12: Key results of the study reproduced using 31 CMIP5 models (RCP8.5 scenario). a) Corresponds to Figure 1c. b) Corresponds to Figure 3a. c) Corresponds to Figure 4b. d) Corresponds to Figure 5c. e) Corresponds to Figure 5e. Generally, CMIP5 results are very similar to those of CMIP6, yet the latter more clearly demonstrate the zonally contrasting shifts of the tropical rainbelt.

Supplementary Table 2: CMIP5 models used to produce Supplementary Figure 12.

	Model	Number of ensembles
1	ACCESS1.0	1
2	ACCESS1.3	1
3	CanESM2	5
4	CMCC-CESM	1
5	CMCC-CM	1
6	CMCC-CMS	1
7	CNRM-CM5	5
8	CSIRO Mk3.6.0	10
9	FGOALS-s2	2
10	GFDL-CM3	1
11	GFDL-ESM2G	1
12	GFDL-ESM2M	1
13	GISS-E2-H	5
14	GISS-E2-H-CC	1
15	GISS-E2-R	1
16	GISS-E2-R-CC	1
17	HadGEM2-CC	2
18	HadGEM2-ES	4
19	INM-CM4	1
20	IPSL-CM5A-LR	4
21	IPSL-CM5A-MR	1
22	IPSL-CM5B-LR	1
23	MIROC5	3
24	MIROC-ESM	1
25	MIROC-ESM-CHEM	1
26	MPI-ESM-LR	3
27	MPI-ESM-MR	1
28	MRI-CGCM3	1
29	MRI-ESM1	1
30	NorESM1-M	1
31	NorESM1-ME	1

References

Adam, O., T. Schneider, F. Brient, and T. Bischoff (2016a) Relation of the double-ITCZ bias to the atmospheric energy budget in climate models, *Geophys. Res. Lett.*, **43**, 7670–7677, doi:10.1002/2016GL069465.

Adam, O., Bischoff, T., & Schneider, T. (2016b). Seasonal and interannual variations of the energy flux equator and ITCZ. Part II: Zonally varying shifts of the ITCZ. *Journal of Climate*, *29*, 7281–7293. https://doi.org/10.1175/JCLI-D-15-0710.1

Adam, O., Schneider, T. & Brient, F. (2018) Regional and seasonal variations of the double-ITCZ bias in CMIP 5 models, *Clim. Dyn*., **51** (101). https://doi.org/10.1007/s00382-017-3909-1

Barimalala, R., Desbiolles, F., Blamey, R. C., & Reason, C. (2018). Madagascar influence on the South Indian Ocean Convergence Zone, the Mozambique Channel Trough and southern African rainfall. *Geophysical Research Letters*, **45**, 11,380-11,389. https://doi.org/10.1029/2018GL079964

Berry, G., & Reeder, M. J. (2014). Objective identification of the intertropical convergence zone: Climatology and trends from the ERA-interim. *Journal of Climate*, **27**, 1894–1909. https://doi.org/10.1175/JCLI-D-13-00339.1

Bischoff, T. and T. Schneider (2016) The equatorial energy balance, ITCZ position, and double-ITCZ bifurcations, *Journal of Climate*, **29**, doi: 10.1175/JCLI-D-15-0328.1

Carvalho, L. M., Jones, C., & Liebmann, B. (2004). The South Atlantic convergence zone: Intensity, form, persistence, and relationships with intraseasonal to interannual activity and extreme rainfall. *Journal of Climate*, **17**, 88–108. https://doi.org/10.1175/1520-0442(2004)017<0088:TSACZI>2.0.CO;2

Cook, K. H. (1998). On the response of the Southern Hemisphere to ENSO. In *Proc 23rd Climate Diagnostics and Prediction Workshop* (pp. 323–326). Miami, FL: American Meteorological Society.

Cook, K. H. (2000). The south Indian convergence zone and interannual rainfall variability over southern Africa. *Journal of Climate*, **13,** 3789–3804. https://doi.org/10.1175/1520-0442(2000)013<3789:TSICZA>2.0.CO;2

Dai, A., and T. M. L. Wigley, (2000) Global patterns of ENSO induced precipitation. *Geophysical Research Letters*, **27**, 1283–1286, doi:10.1029/1999GL011140.

Dutheil, C., et al., (2019) Impact of temperature biases on climate change projections of the South Pacific Convergence Zone, *Climate Dynamics*, https://doi.org/10.1007/s00382-019-04692-6

Haffke, C., & Magnusdottir, G. (2013). The South Pacific convergence zone in three decades of satellite images. *Journal of Geophysical Research: Atmospheres*, **118**, 10839–10849. https://doi.org/10.1002/jgrd.50838

Haffke, C. and G. Magnusdottir (2015) Diurnal cycle of the South Pacific Convergence Zone in 30 years of satellite images, *Journal of Geophysical Research: Atmospheres*, **120**, 9059-9070

Haffke, C., G. Magnusdottir, D. Henke, P. Smyth, Y. Peings (2016) Daily states of the March-April east Pacific ITCZ in three decades of high-resolution satellite data, *Journal of Climate*, **29**, 2981-2995. doi: 10.1175/JCLI-D-15-0224.1

Hwang, Y., and D. Frierson (2013) Link between the double-intertropical convergence zone problem and cloud biases over the Southern Ocean. *Proc. Natl. Acad. Sci. USA*, **110**, 4935–4940.

Li, G., and Xie, S.-P. (2014) Tropical Biases in CMIP5 Multimodel Ensemble: The Excessive Equatorial Pacific Cold Tongue and Double ITCZ Problems, *J. Clim.*, **27**, 1765–1780.

Mamalakis, A., & Foufoula-Georgiou, E. (2018). A multivariate probabilistic framework for tracking the intertropical convergence zone: Analysis of recent climatology and past trends. *Geophysical Research Letters*, **45**, 13,080-13,089. https://doi.org/10.1029/2018GL079865

Mechoso, C., and Coauthors (1995) The seasonal cycle over the tropical Pacific in coupled ocean–atmosphere general circulation models. *Mon. Wea. Rev.*, **123**, 2825–2838.

Oueslati, B. and Bellon, G., (2015) The double ITCZ bias in CMIP5 models: interaction between SST, large-scale circulation and precipitation, *Climate Dynamics*, **44**, 585–607, doi:10.1007/s00382-015- 2468-6.

Pauluis, O., (2004) Boundary Layer Dynamics and Cross-Equatorial Hadley Circulation, Journal of the Atmospheric Sciences, **61**, 1161-1173.

Samanta, D., Karnauskas, K. B., & Goodkin, N. F. (2019). Tropical Pacific SST and ITCZ biases in climate models: Double trouble for future rainfall projections?. *Geophysical Research Letters*, **46**, 2242-2252. https://doi.org/10.1029/2018GL081363

Tian, B., & Dong, X. (2020) The double-ITCZ Bias in CMIP3, CMIP5 and CMIP6 models based on annual mean precipitation, *Geophysical Research Letters*, **47**, e2020GL087232. https://doi.org/10.1029/2020GL087232

Widlansky, M. J., Webster, P. J., & Hoyas, C. D. (2011). On the location and orientation of the South Pacific Convergence Zone, *Climate Dynamics*, **36**, 561–578. https://doi.org/10.1007/s00382-010-0871-6

Waliser, D. E. & Gautier, C. (1993) A satellite-derived climatology of the ITCZ. *Journal of Climate*, **6**, 2162–2174.

Yang, W. and G. Magnusdottir (2016) Interannual signature in daily ITCZ states in the east Pacific in boreal spring, *Journal of Climate*, **29**, 8013-8025. doi: 10.1175/JCLI-D-16-0395.1